3. Energetics of the ultrafast associative desorption of hydrogen from Ru(001)

This chapter provides the results concerning the energetics of the femtosecond-laser induced associative desorption of hydrogen from a saturation covered Ru(001) surface. (Note that in the following the notation hydrogen is used for both isotopes, H and D, as long as there is no loss of generality.) A first section gives an overview over the adsorbate system H/Ru(001) and the hot electron mediated reaction mechanism. The results revealing the energy transfer into the different molecular degrees of freedom are presented afterwards. A very detailed discussion concentrating on the experimentally gained microscopic understanding of the investigated process follows. The still remaining open questions are then discussed separately in the light of very recent theoretical investigations which complete the knowledge about the fs-laser induced associative desorption of hydrogen from Ru(001).

3.1. Introduction to the current research status

Before presenting results concerning the energetics of the fs-laser induced associative desorption from a Ru(001) surface, an overview over the current research status will be given. This includes an overview concerning the well studied adsorbate system hydrogen on ruthenium (Section 3.1.1) and summarizes the investigations performed by Denzler et al. [Den03a, Den03b, Den04] which reveal the electron mediated reaction mechanism of the fs-laser induced desorption.

3.1.1. The adsorbate system H/Ru(001)

Because of its simplicity, molecular hydrogen often serves as a model system for the investigation of molecule-surface interactions. This and its particular importance for catalytic reactions [Sto51] account for the large number of investigations concerning the adsorbate system hydrogen on Ru(001).

H_2 adsorbs dissociatively on Ru(001) [Shi80b]. In an early study, Feulner and Menzel [Feu85] interpreted an observed coverage dependent workfunction and sticking coefficient as an indication for two different adsorption states. Lindroos et al. revealed [Lin87b] that this behavior is not because of different bonding sites, but due to adsorbate-adsorbate interactions. It was found that hydrogen adsorbs on the *fcc* hollow sites throughout the whole coverage range [Hof85, Lin87a, Lin87b, Sok91], with a saturation coverage corresponding to $\theta = 1\,\mathrm{ML}$ [Sun89]. Such a saturation covered (1×1)-H:Ru(001) structure is depicted in the inset of Fig. 3.1(b). The adsorption at *fcc* sites is energetically more favorable than *hcp* sites as revealed by theoretical investigations [Cho87, Cho89, Fei94, Xu05]. The energetic difference of $\approx 0.05\,\mathrm{eV}$

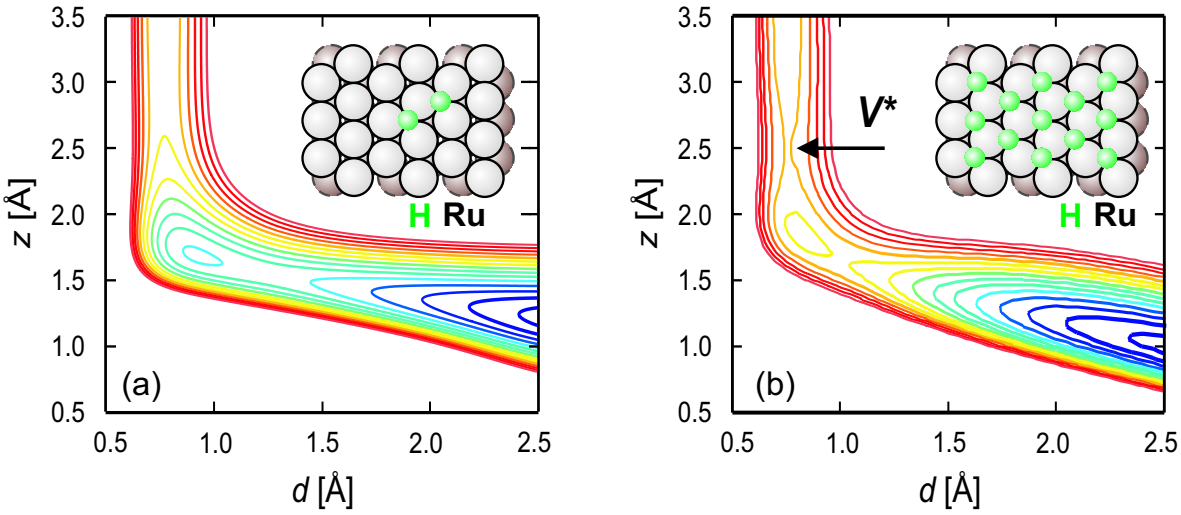

Figure 3.1.: Contour plots of DFT PESs governing the H_2 adsorption on Ru(001) as function of the molecular stretch d and the center-of-mass to surface distanze z. (a) 2D cut through the 6D PES computed for a molecule interacting with a bare surface is depicted. (b) 2D PES for the desorption from a hydrogen covered surface is shown. Note the appearance of a translational barrier of height $V^* \approx 60\,\text{meV}$ at the PES mapped on the right indicated by an arrow. Contours are at 0.1 eV. Figures taken with courtesy of M. Luppi and A.C. Luntz from [Lup] and [Lun06], respectively.

between those two sites is almost independent on coverage, whereas the absolute adsorption energy is not [Xu05]. If the substrate is covered with only half a monolayer ($\theta = 0.5\,\text{ML}$), the hydrogen atoms are more strongly bound ($E_{\text{ads}} \approx 0.6\,\text{eV/atom}$) than at saturation coverage $\theta = 1\,\text{ML}$, where the adsorption energy E_{ads} is $\approx 0.5\,\text{eV/atom}$ [Feu85, Xu05]. This behavior is again contributed to the above mentioned adsorbate-adsorbate interactions.

Figure 3.1 shows potential energy surfaces (PESs) for the H_2 molecule interacting with a Ru(001) surface. The PESs are obtained from DFT calculations performed by Luppi et al. [Vin05, Lup] and Luntz et al. [Lun06] who both use the same DFT functional. Luppi et al. performed a 6D calculation considering the interaction of molecular hydrogen with a clean Ru(001) surface. An elbow plot based on the 6D PES for the most reactive molecular configuration is shown on the left of Fig. 3.1. The barrier to adsorption on this bare surface is $V^* = 12\,\text{meV}$ [Vin05, Lup][1]. On the right hand side, a 2D PES for the adsorption on a hydrogen covered Ru(001) surface is depicted. A barrier to adsorption of $V^* \approx 60\,\text{meV}$ relative to the H_2+Ru:H asymptote is observable [Lun06]. This means that V^* increases with hydrogen coverage. The increasing barrier height is consistent with the decrease in thermal H_2 sticking on Ru(001) observed experimentally for a hydrogen coverage close to saturation $\theta \sim 1\,\text{ML}$ [Feu85].

To complete the information obtainable from the 6D PES calculations, the most reactive molecular configuration is noted: the molecule is oriented parallel to the surface with the center of mass at the *top* site. Only very little anisotropy is found for the minimum energy along the reaction path with respect to the azimuthal angle [Vin05]. The 2D calculations performed by Luntz et al. are based on this minimum barrier configuration [Lun06].

[1] Note that a higher barrier of 85 meV is predicted by the same group using another DFT functional for H_2/Ru(001) [Vin05, Lup]. This is inconsistent with the high initial sticking coefficient of H_2 on a bare Ru(001) observed in experiments [Feu85].

3.1.2. The femtochemistry

Denzler et al. investigated the fs-laser induced desorption of hydrogen from a hydrogen covered Ru(001) surface in great detail and found an electron mediated reaction mechanism [Den03b, Den04]. The essential experimental findings will be summarized in a brief overview:

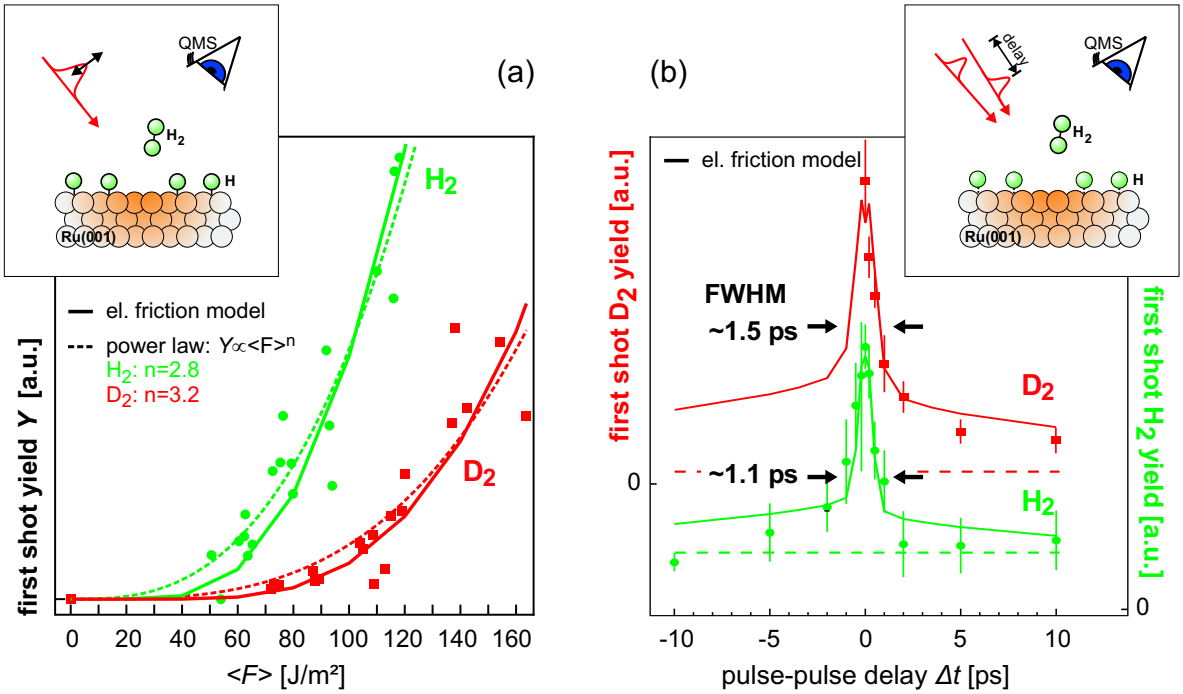

Figure 3.2.: (a) Fluence dependence of the H_2 and D_2 first-shot desorption yield from a saturation coverage of the respective isotope. The dashed lines show the fit by a power law $\langle F\rangle^n$ with $n = 2.8$ and $n = 3.2$ for H_2 and D_2, respectively. (b) 2PC measurement for hydrogen and deuterium desorption yields. For clarity, the D_2 data is offset vertically. The dashed lines represent the desorption yield for two pulses in the limit of infinite temporal separation. FWHM of ≈ 1.1 and ≈ 1.5 ps for H_2 and D_2, respectively, reveal an electron mediated reaction mechanism. (a)+(b) Solid lines represent the outcome of the friction model explained in Section 1.3. Figures taken from [Den03a].

The first shot yield Y as a function of absorbed laser fluence[2] $\langle F\rangle$ is depicted in Fig. 3.2(a). A non-linear dependence is observed. The dependency can be described by a power law $Y \propto \langle F\rangle^n$ with $n \approx 3$. The deviations of $n = 2.8$ for H_2 and $n = 3.2$ for D_2 are within the error bars. The non-linearity is a clear indication for a multiple excitation process driving the reaction, since a single excitation process would result in a linear fluence dependence. An isotope effect showing higher reaction yields for the lighter isotope is obvious and will be discussed in Section 3.3.

The non-linear fluence dependence allows to perform a 2PC measurement (see Section 1.3.4). Two laser pulses are delayed in time and the desorption yield Y is measured as a function of the delay Δt. The absorbed fluence of both pulses is $120\,\mathrm{J/m^2}$ with an intensity ratio for the two pulses of 54:46. The 2PCs for the two isotopes are shown in Fig. 3.2(b). The dashed line represents the desorption yield for two laser pulses separated "infinitely" in time. The

[2] $\langle F\rangle$ denotes the yield weighted fluence, which considers the non-linearity of the reaction mechanism and the spatial energy distribution of the laser pulse as explained in Section 2.5.

measured narrow full width at half maximum (FWHM) of ≈ 1.1 and ≈ 1.5 ps for H_2 and D_2, respectively, means that only at delays smaller than $\approx \pm 1$ ps the second laser pulse benefits drastically from the excitation by the first pulse. This short energy storage time identifies unambiguously an electron mediated reaction mechanism (Section 1.3.4).

The experimental data is well reproduced within the framework of the applied frictional approach for modeling the adsorbate-substrate coupling introduced in Section 1.3. The coupling depends on the transient electron and phonon temperatures T_{el} and T_{ph} calculated with the two-temperature model (Section 1.2). The outcome of the modeling is depicted by solid lines in Fig. 3.2. A single parameter set is sufficient to well reproduce the fluence dependence, the isotope effect and the 2PCs. The best fit yields an activation energy $E_{\mathrm{a}} = 1.35$ eV and inverse coupling times $\eta_{\mathrm{el,H_2}} = 1/180\,\mathrm{fs}^{-1}$ and $\eta_{\mathrm{el,D_2}} = 1/2 \cdot \eta_{\mathrm{el,H_2}} = 1/360\,\mathrm{fs}^{-1}$ for H_2 and D_2, respectively. The ratio of a factor of two regarding η_{el} for the two isotopes can be rationalized by Eq. (1.45), which considers the mass-dependent acceleration from the same frictional force.

Summarizing one can say that a clear experimental indication for a non-adiabatic reaction mechanism driven by hot substrate electrons is found for the fs-laser induced desorption of hydrogen from Ru(001).

Further interesting peculiarities like a threshold-like coverage dependence of the desorption yield [Den04] and promotion effects in isotopically substituted surrounding of the reactants [Den03b] have been found, but are beyond the scope of this brief introduction. Furthermore, TOF measurements revealed high translational energies for desorbing hydrogen molecules, but no systematic investigation was possible because of an insufficient experimental time resolution [Den03b]. Thus, the energy content in the desorbing particle flux, especially the energy transfer into the internal molecular degrees of freedom, remains unknown.

3.2. Experimental results: the energetics of the desorption process

The outcome of the experimental investigations concerning the energy transfer into the different molecular degrees of freedom of desorbing hydrogen molecules after fs-laser irradiation of a saturation covered H/Ru(001) surface will be presented. The section is divided into three parts. In a first part, the non-state-selective time-of-flight measurements are shown. Therefrom, information about the translational energies are deduced. Knowledge about the energy transfer to the internal molecular degrees of freedom is obtained from measurements of the rovibrational state distribution, which is subject of the second part. The final part also concerns the determined molecular alignment and ends the section.

3.2.1. Time-of-flight measurements

The time-of-flight (TOF) measurements have been performed with an experimental setup described in Section 2.5.1. Recorded TOF distributions of D_2 for various absorbed laser fluences $\langle F \rangle$ are depicted in Fig. 3.3. The laser fluence ranges from 50 to 140 J/m^2. The analysis of the obtained data is explained in detail in Section 2.4.2. The mean translational energy $\langle E_{\mathrm{trans}} \rangle$ along the direction of the surface normal is obtained from the second moment of the experimental data and expressed in terms of a translational temperature $T_{\mathrm{trans}} = \langle E_{\mathrm{trans}} \rangle / 2k_{\mathrm{B}}$. Each TOF distribution can be described very well by a single modified Maxwell-Boltzmann distributions represented by solid lines in Fig. 3.3. The descriptiveness of the spectra with single Maxwell-Boltzmann distributions suggests that the desorption occurs via a single reaction channel and allows to describe the measured TOF distribution with one temperature. In the present case of D_2, translational temperatures range from 2000 to 3200 K. A shift to shorter flight times with increasing laser fluence, as obvious from Fig. 3.3, corresponds to an increase in T_{trans}.

In Fig. 3.4, two exemplary TOF distributions for H_2 and D_2 are depicted. The absorbed laser fluences $\langle F \rangle$ of 60 and 70 J/m^2 for the H_2 and D_2 formation are comparable. Despite the slightly lower absorbed fluence, a shorter flight time $\langle t \rangle$ is measured for the lighter isotope. As obvious from $\langle t \rangle \propto \langle v \rangle^{-1} \propto [\langle E \rangle / m]^{-1/2}$, a shorter flight time corresponding to a higher velocity $\langle v \rangle$ can either result from the smaller particle mass m or an increased translational energy $\langle E \rangle$. To distinguish these two contributions, a modeled TOF distribution for H_2 exhibiting the same kinetic energy as the measured D_2 data is plotted as a dashed curve in the upper panel of Fig. 3.4. Therefrom and from the vertical dashed lines, it is obvious that both effects contribute to the shorter flight time. Δt_{m} denotes the difference due to the lighter mass, whereas $\Delta t_{\langle E \rangle}$ represents the shift due to a higher kinetic energy. This means a pronounced isotope effect concerning $\langle E \rangle$ is found.

The mean translational energies $\langle E_{\mathrm{trans}} \rangle / 2k_{\mathrm{B}} = T_{\mathrm{trans}}$ of H_2 and D_2 leaving the Ru(001) surface after fs-laser irradiation are depicted in Fig. 3.5 as a function of absorbed laser fluence $\langle F \rangle$. Increasing laser fluence $\langle F \rangle$ leads to an increase in $\langle E_{\mathrm{trans}} \rangle$ by $\approx 60\%$ within the applied fluence range. Concerning the isotope effect, applying same fluences $\langle F \rangle$ leads to differences of ≈ 1000 K in T_{trans} with higher kinetic energies for the lighter isotope. It should be noted that in earlier experiments performed by Denzler et al. [Den03b], neither the isotope effect nor the fluence dependence were observable due to the limited temporal resolution in their TOF spectra.

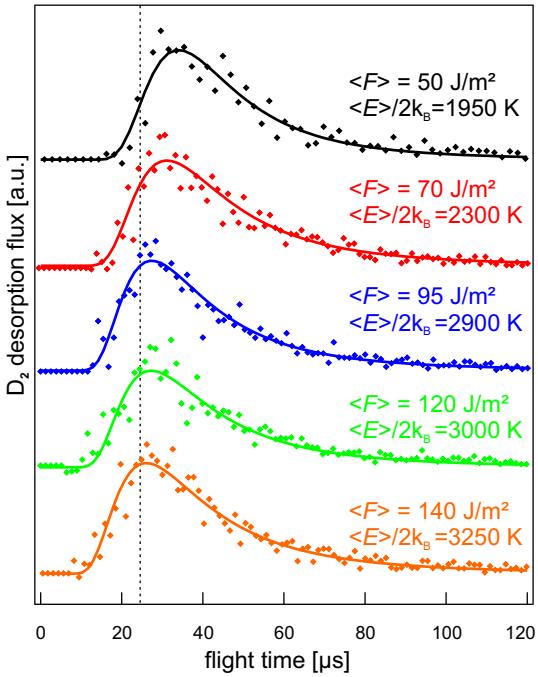

Figure 3.3.: TOF distributions of desorbing D_2 after fs-laser irradiation of a saturation covered D/Ru(001) surface. The absorbed laser fluence $\langle F \rangle$ ranges from 50 to 140 J/m^2. The dashed line is a guide to the eye to clarify the decrease in flight time with increasing fluence. Solid lines are modified Maxwell-Boltzmann distributions for the corresponding temperatures $\langle E \rangle / 2k_B$.

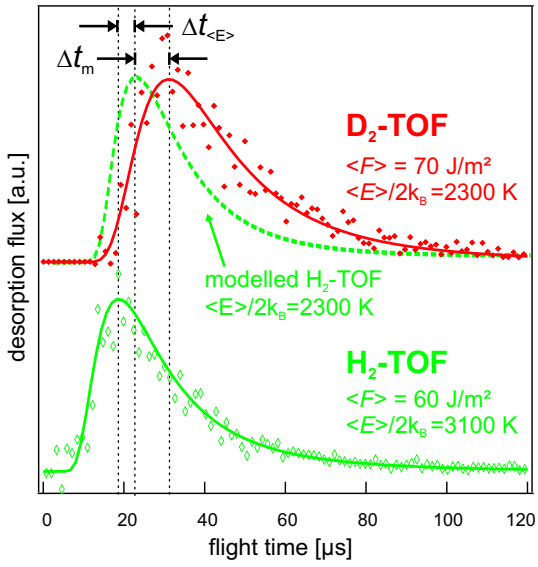

Figure 3.4.: TOF distributions of desorbing H_2 (lower panel) and D_2 (upper panel) after fs-laser induced recombinative desorption. The absorbed laser fluences $\langle F \rangle$ of 60 and 70 J/m^2 for the H_2 and D_2 case, respectively, are comparable. The shorter flight times for the H_2 molecules result from the lighter molecule mass and a higher translational energy which is visualized by the vertical dashed lines and a modeled Maxwell-Boltzmann distribution for H_2 exhibiting the same $\langle E \rangle$ as the measured D_2 data (dashed curve, upper panel).

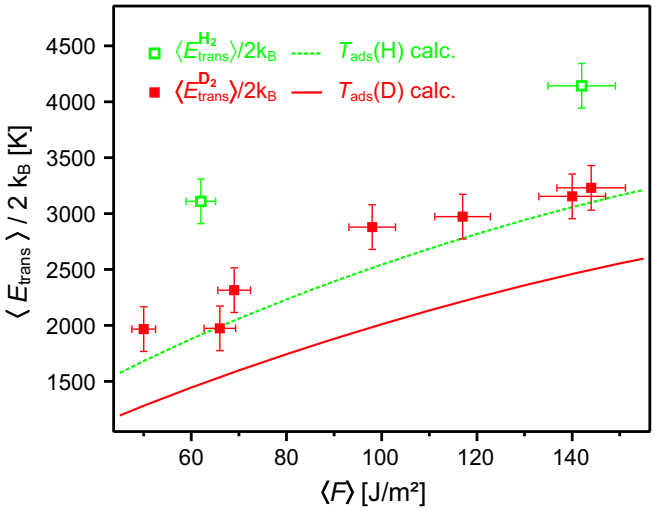

Figure 3.5.: Mean translational energies $\langle E \rangle / 2k_B$ of H_2 and D_2 desorbing after fs-laser irradiation of a saturation covered Ru(001) surface are depicted as a function of absorbed laser fluence $\langle F \rangle$. The lines represent calculated rate-weighted adsorbate temperatures T_{ads}^{RW}. Solid line and symbols correspond to deuterium and dashed lines and opened symbols to hydrogen, respectively.

In addition to the experimental data, rate-weighted adsorbate temperatures T_{ads}^{RW} are plotted as a function of laser fluence $\langle F \rangle$ as solid and dashed line in Fig. 3.5. To obtain T_{ads}, the energy flow after fs-laser excitation between substrate and adsorbate is modeled within the framework of a frictional approach (Section 1.3) and the parameter set (η_{el,D_2}, E_a) specified in Section 3.1.2 is applied. T_{ads}^{RW} is then calculated via

$$T_{ads}^{RW} = \frac{\int R(t) \cdot T_{ads}(t)\,dt}{\int T_{ads}(t)\,dt}, \tag{3.1}$$

where the desorption rate $R(t)$ and the transient adsorbate temperature $T_{ads}(t)$ are given by Eq. (1.42) and Eq. (1.33), respectively. As can be seen from Fig. 3.5, the trends of the fluence dependence and isotope effect are well reproduced, although an offset between modeled and measured temperatures has to be stated. This difference will be discussed in Section 3.3.

To distinguish influences from the ground state PES governing the desorption and from the fs-laser excitation, the data is linearly extrapolated towards zero fluence which neglects laser excitation. The axis intercept at $\langle F \rangle = 0$ of $\approx 1250\,K$ (corresponding to $\approx 200\,meV$) yields information about the minimum energy released into the translational degrees of freedom of the desorbing molecules and constitutes thus an conservative upper bound for a translational barrier, as will be discussed in Section 3.3.

3.2.2. Rovibrational state distribution and molecular alignment

Information about the energy transfer into the internal molecular degrees of freedom of desorbing D_2 molecules is obtained by state-resolved detection via the resonance enhanced multi-photon ionization (REMPI) described in Section 2.4.3 using the experimental setup introduced in Section 2.4.3 and Section 2.5.1.

The REMPI ion signal of D_2 molecules formed after fs-laser irradiation of a saturation covered D/Ru(001) surface is depicted in Fig. 3.6 as a function of excitation wavelength λ_{VUV}. The

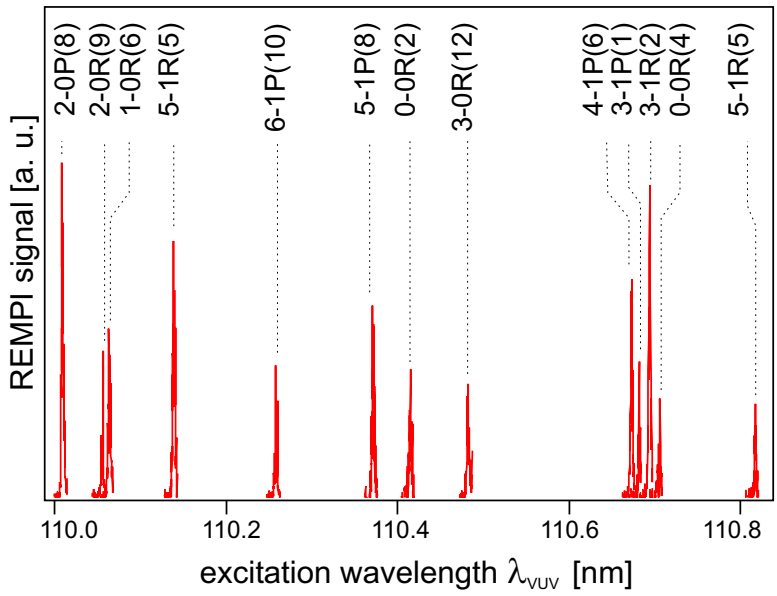

Figure 3.6.: REMPI spectrum of D_2 molecules desorbing from deuterium saturation covered Ru(001) surface after fs-laser excitation with $85\,\mathrm{J/m^2}$ absorbed fluence as a function of excitation wavelength λ_{VUV}. The notation of the resonances is given in Section 2.4.3.

absorbed laser fluence is $\langle F \rangle = 85\,\mathrm{J/m^2}$. Various, clearly distinguishable resonances in the Lyman (0-0) to (3-0) and (3-1) to (6-1) bands are depicted. D_2 molecules in vibrational states of $v'' \geq 2$ could not be detected in the experiment. The REMPI signal is transformed into a rovibrational state distribution via Eq. (2.14) and Eq. (2.15). The transition probabilities for the probed resonances are known from studies by Wetzig et al. [Wet01] and Rutkowski et al. [Rut02b]. The so-obtained rotational state populations of the desorbing D_2 are normalized with respect to the statistical weight $(2J''+1)g_{\mathrm{n}}$ with g_{n} allowing for the different spin multiplicity of ortho- versus para-type D_2. In Fig. 3.7, the normalized population distributions for the vibrational ground state and the first excited state are plotted in a semi-logarithmic plot versus the rotational energy E_{rot} and the total internal energy $E_{\mathrm{rot}} + E_{\mathrm{vib}}$, where E_{vib} denotes the vibrational energy. For a completely thermalized ensemble, such a Boltzmann plot for a population distribution would exhibit a linear slope proportional to $1/T_{\mathrm{rot}}$. As obvious from Fig. 3.7, this is not the case for the rotational ground state distribution. States with $J'' \leq 6$ show a distinct higher occupation. Nevertheless, one can still express the energy content in the $v''=0$ in terms of $\left\langle E_{\mathrm{rot}}^{v''=0} \right\rangle / k_{\mathrm{B}} = 800\,\mathrm{K}$. The data obtained for the vibrationally excited $v''=1$ state exhibits a thermal distribution, which can be described by a rotational temperature of $T_{\mathrm{rot}} = \left\langle E_{\mathrm{rot}}^{v''=1} \right\rangle / k_{\mathrm{B}} = 1500\,\mathrm{K}$.

Having a look at Fig. 3.7(b), where the population distributions are plotted against the internal energy of the D_2 molecules, one notices that no vertical offset is observed between the vibrational states $v''=0$ and $v''=1$. The Boltzmann plot of the two distributions exhibits the same linear slope for internal energies larger than $2000\,\mathrm{cm^{-1}}$. In the energy range from 3000 to $4500\,\mathrm{cm^{-1}}$, where states in $v''=0$ and $v''=1$ overlap, no preferential energy coupling into one of the two involved vibrational states is observed. Over the entire range of internal energy, the measured rovibrational distribution can be fitted by the sum of two almost equally populated Boltzmann distributions of temperatures $T_1 = 370\,\mathrm{K}$ and $T_2 = 1500\,\mathrm{K}$. Considering

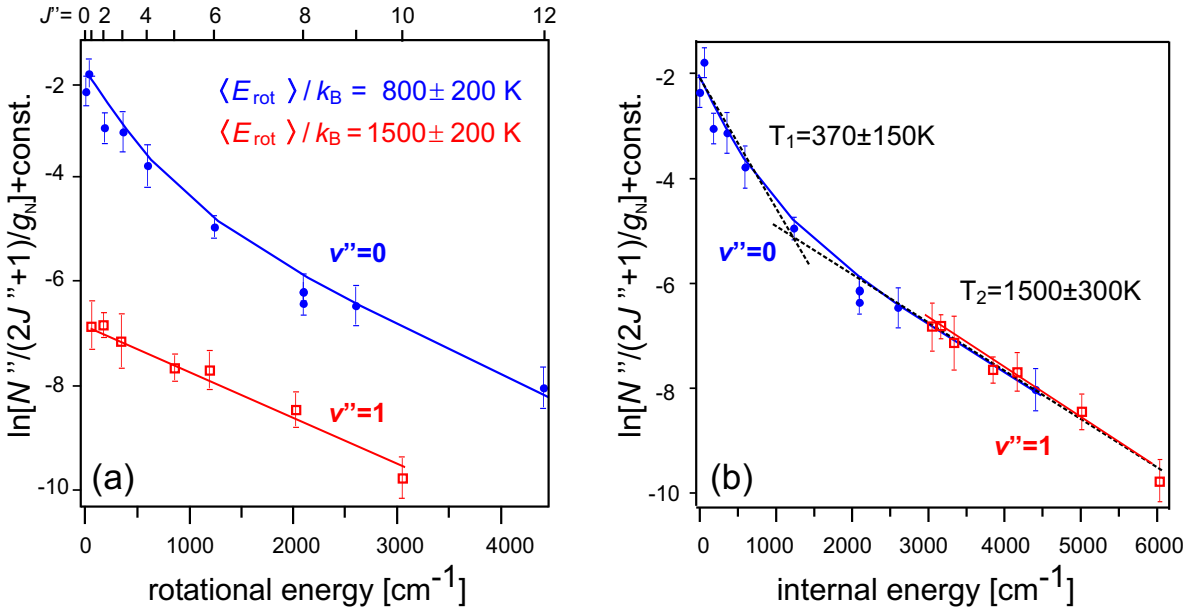

Figure 3.7.: Rovibrational population distributions $N(v'', J'')$ of D_2 desorbing from Ru(001) after fs-laser excitation with $\langle F \rangle = 85\,\mathrm{J/m^2}$. Boltzmann plots for the vibrational ground and first excited state are shown versus the rotational energy (a) and the total internal energy (b).

the descriptiveness of the experimental data by two thermalized Boltzmann distributions, one is tempted to interpret this finding as an evidence for two thermalized independent reaction channels with different mechanisms and energetics. However, such a scenario can be ruled out by taking the TOF spectra depicted in Section 3.2.1 into account. These are very well reproduced by *single* Maxwell-Boltzmann distributions which is contradictory to two thermalized distributions with 370 and 1500 K, respectively.

To express the overall energy content in the rotational degrees of freedom, one can derive a *mean* rotational temperature $T_{\mathrm{rot}} = 910\,\mathrm{K}$ by weighting the temperatures obtained for the two Boltzmann distributions by their population. This only means that the energy content can be described by a single temperature but not the rovibrational distribution itself. Under the assumption that the vibrational quantum states are populated in a Boltzmann-like behavior, the energy content of the vibrational degree of freedom can be given by a *mean* vibrational temperature of $T_{\mathrm{vib}} = 1200 \pm 250\,\mathrm{K}$. This procedure seems plausible since the measured TOF distributions and the measured rovibrational state distribution can be well described by single or two temperatures, respectively. In addition, the non-observed population of $v'' = 2$ states is consistent with this assumption. For the electron stimulated desorption (ESD) with electron energies of 150 eV of CO molecules from Ru(001), Wurm et al. observed extremely high vibrational excitation with inverted Boltzmann distributions [Wur95, Wur98]. This completely non-thermal behavior is contributed to resonant multi-electron excitation involving inner valence states of the CO molecule [Wur95]. Thus, for the present experiment with photon energies of 1.55 eV and atomically bound hydrogen we exclude a similar behavior and believe that the assumption of a thermalized vibrational state distribution represents the energy content in the vibration to an adequate accuracy.

Molecular Alignment

As explained in detail in Section 2.4.3, the experimental setup offers the possibility to measure the molecular alignment of the desorbing D_2 molecules. Our results of the rotational alignment for several rovibrational states and laser fluences reveal neither a dependence on the laser fluence nor on the quantum state. Nevertheless, a significant positive alignment was found exemplified for the (2-0P8) transition with $A_0^{(2)} = 0.27 \pm 0.15$. $A_0^{(2)}$ defines a distribution $\sigma(m_J)$, where m_J denotes the projection of J'' onto the surface normal. A $\sigma(m_J)$ distribution corresponding to an alignment of $A_0^{(2)} = 0.27$ is depicted in Fig. 2.16, Section 2.4.3. This distribution implies that about three quarters, $(74 \pm 6)\,\%$, of the molecules desorb with $|M_{J''}| \geq J''/2$, i.e. in a more helicopter-like rotation, and one quarter, $(26 \pm 6)\,\%$, with $|M_{J''}| < J''/2$.

3.2.3. Possible distortions of the rovibrational state distribution due to gas phase collisions

Before relating the characterization of the D_2 desorption flux to the underlying surface reaction, it is important to assure that the experimental data represents the initial status resulting from the reaction and are not distorted due to gas phase collisions before detection. Such collisions may lead to a decay of the molecular alignment and a thermalization of the population distribution. For hydrogen molecules, both H_2 and D_2, the number of collisions required for significant rotational energy transfer ranges from 100 to 1000 [Rab75, Lam77, Mei86], whereas even 10^4 to 10^5 collisions are required for vibrational relaxation [Lam77]. Although no investigations of the alignment decay for D_2 are known, experiments performed by Halpern et al. [Hal95] investigating the C_2H_2 molecule show that rotational alignment decay is significantly slower than the rotational population decay. This should also be valid for D_2 molecules, which even have a smaller bond length than C_2H_2 and thus appear more spherical and less prone to alignment quenching interactions.

The number of molecules desorbing per laser shot is known from measurements, where the desorption yield is measured as a function of the shot number of the laser irradiating the same spot on the sample. Such depletion curves are depicted in Fig. 3.8 for several applied laser fluences $\langle F \rangle$. The higher the fluence the less laser shots are required to deplete the surface. This is in accordance with the non-linear fluence dependence depicted in Fig. 3.2, Section 3.1.2. Desorption only takes place for coverages $\theta \geq 0.5\,\mathrm{ML}$ [Den04], which means that the integrated depletion curve corresponds to a coverage of $\theta \approx 0.5\,\mathrm{ML}$. Thus, the maximum D_2 flux for the first laser shot is known. For $\langle F \rangle = 85\,\mathrm{J/m^2}$, the fluence applied for the state-resolved experiments, a D_2 flux of $\approx 1{\cdot}10^{13}/\mathrm{cm^2}$ has to be considered.

Monte-Carlo simulations performed by NoorBatcha et al. [Noo87] model the effect of gas-phase collisions on NO molecules which rapidly desorb from a LiF(100) surface due to laser induced desorption. The particle flux in the D_2 desorption experiments is comparable to that of $0.6 \cdot 10^{13}/\mathrm{cm^2}$ considered in their calculations and the collision cross section for NO is a factor of two larger than the one for D_2 [Cow78, Noo87]. Although the desorption time is varied by three orders of magnitude, only a small variation of the collision probability is found [Noo87]. Comparing this with the number of collisions required for significant distortion of the nascent D_2 desorption flux leads to the conclusion that our experimental data can be exclusively related to the surface reaction under investigation.

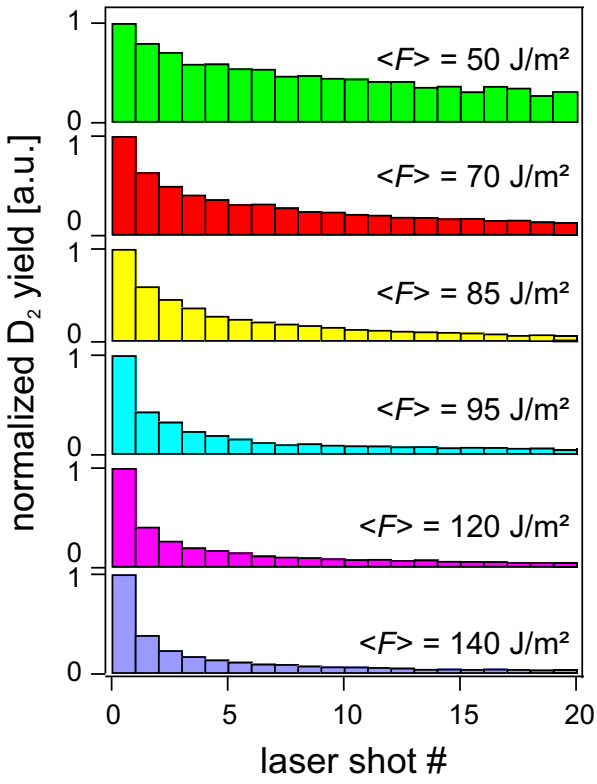

Figure 3.8.: Depletion curves of normalized D_2 yield from (1×1) coverages for various fluences as a function of laser shot number. The higher the laser fluence $\langle F \rangle$ the less laser shots are required to deplete the surface.

This is additionally corroborated by several experimental facts: First of all, a non-thermalized rovibrational state distribution is measured with an overpopulation of low J'' in $v'' = 0$ neglecting a possible rotational decay leading to thermalization. In addition a non-zero molecular alignment is found. Last but not least, no narrowing of the TOF distributions with increasing laser fluence is observed. Since the cross sections for translational-translational, translational-rotational and translational-vibrational energy transfer relate as $\sigma_{\text{t-t}} \gg \sigma_{\text{r-t}} \gg \sigma_{\text{v-t}}$, a narrowing of the TOF spectra depicted in Fig. 3.3 with increasing particle density, i.e. with higher laser fluences $\langle F \rangle$, would be expected if collisions played a crucial role after desorption. Such a nozzling effect however, is not observed in the experiment performed.

Both, experimental findings and theoretical considerations lead to the conclusion that the experimental findings are not changed by gas phase collisions and can therefore be directly related to the desorption process.

3.3. Discussion of the experimental results

Having gained information about the energy content in the desorbing D_2 particle flux, knowledge about the fs-laser excited deuterium covered Ru(001) surface is required to interpret the measured data. The excitation of the metal surface is described with the two-temperature model (2TM) introduced in Section 1.2, and the energy transfer into the adsorbate is modeled in a frictional approach explained in Section 1.3.

Rate-weighted adsorbate temperature

The transient electron and phonon temperatures T_{el} and T_{ph} of the Ru(001) surface as well as the adsorbate temperature T_{ads} after fs-laser excitation are depicted in Fig. 3.9. The fit parameters denoted in Section 3.1.2 are applied for the modeling. In addition, the transient reaction rate is shown and its integration over time results in the desorption yield. As can be seen, $T_{\mathrm{ads}}(t)$ follows the electronic temperature with a certain time delay and reaches its maximum at $\approx 400\,\mathrm{fs}$ after the laser pulse strikes the Ru(001) surface. To get from the transient adsorbate temperature $T_{\mathrm{ads}}(t)$ to a single temperature representing the adsorbate heat bath, a rate-weighted adsorbate temperature $T_{\mathrm{ads}}^{\mathrm{RW}}$ is used as already defined by Eq. (3.1) in Section 3.2.1. This means that $T_{\mathrm{ads}}(t)$ contributes to $T_{\mathrm{ads}}^{\mathrm{RW}}$ according to its respective reaction rate $R(t)$. For a fluence of $\langle F \rangle = 85\,\mathrm{J/m^2}$ applied in the state selective REMPI experiments, a $T_{\mathrm{ads}}^{\mathrm{RW}} = 1800\,\mathrm{K}$ is obtained.

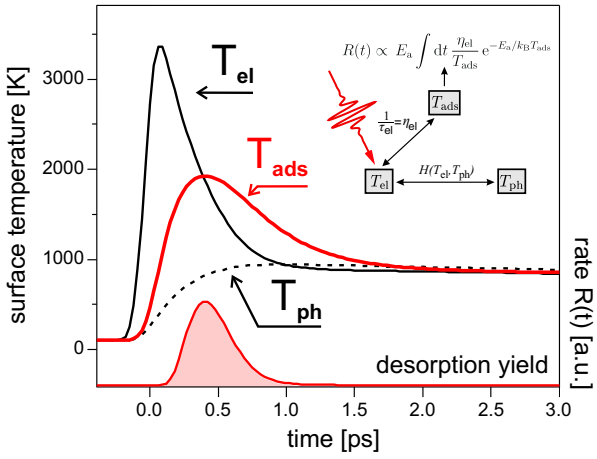

Figure 3.9.: Time profiles of electronic and phononic temperatures T_{el} and T_{ph} of the Ru surface together with the adsorbate temperature T_{ads} of a D adlayer and its respective reaction rate $R(t)$ after fs-laser excitation with $\langle F \rangle = 85\,\mathrm{J/m^2}$. The parameter set obtained in Section 3.1.2 is used for purely electronic frictional coupling as schematically depicted in the inset.

Isotope effect

The pronounced isotope effect concerning the translational energies $\langle E_{\mathrm{trans}} \rangle$ of the desorbing hydrogen molecules after fs-laser induced recombinative desorption is qualitatively well reproduced by the friction model as shown in Fig. 3.5. The transient adsorbate temperatures $T_{\mathrm{ads}}(\mathrm{H_2})$ and $T_{\mathrm{ads}}(\mathrm{D_2})$ for the two isotopes after fs-laser excitation with $\langle F \rangle = 70\,\mathrm{J/m^2}$ are depicted in the left of Fig. 3.10. A faster rise to higher adsorbate temperatures for the lighter isotope can be seen. This is due to the twice as large coupling coefficient $\eta_{\mathrm{el,H_2}} = 2 \cdot \eta_{\mathrm{el,D_2}}$ governing the energy transfer between electron and adsorbate heat baths (Section 3.1.2). The more efficient heating of the H adlayer compared to its heavier counterpart D results in higher adsorbate temperatures, which might be responsible for a desorbing particle flux with higher translational energy $\langle E_{\mathrm{trans}} \rangle$. In addition, the higher adsorbate temperature for H leads also to a higher desorption yield as can be seen from Fig. 3.10. This effect was experimentally investigated by Denzler et al. [Den03b] and is illustrated in Fig. 3.2.

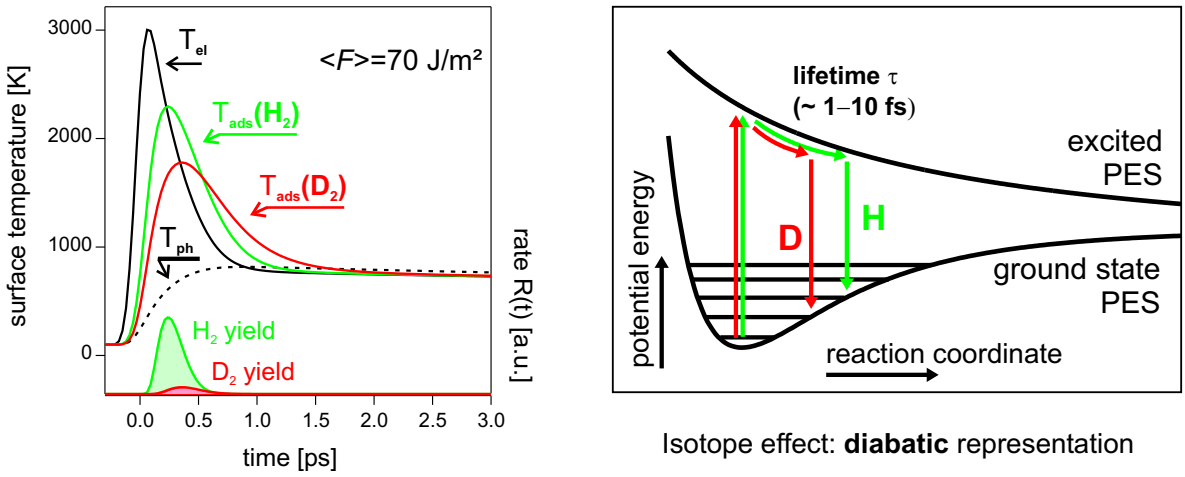

Figure 3.10.: Left: Time profiles of the temperatures T_{el}, T_{ph} and T_{ads} characterizing the corresponding electron, phonon and adsorbate heat baths after fs-laser excitation of a hydrogen saturation covered Ru(001) surface with $\langle F \rangle = 70\,\mathrm{J/m^2}$. Adsorbate temperatures T_{ads} and desorption rates $R(t)$ are plotted for the two investigated hydrogen isotopes. Higher adsorbate temperatures and a higher reaction yield are obtained for the lighter isotope. Right: Illustration of the enhanced energy transfer into the lighter isotope in the framework of the diabatic representation.

Formally, the isotope effect results from a mass-independent frictional force accelerating adsorbates of different masses. A more depictive way of explanation is illustrated on the right hand side of Fig. 3.10. In the diabatic representation of electron mediated surface reactions, the electronic excitation is represented by a transition to a higher-lying electronically excited PES. The gradient of this potential accelerates the adsorbate. The lighter adsorbate is accelerated more strongly and therefore travels a larger distance before electronic de-excitation and thus return to the ground state PES occur. After such an excitation cycle, the lighter isotope has gained more energy than its heavier cousin. Since the topology of the excited PES only depends on the electronic configuration, its gradient also represents a mass-independent force as used in the adiabatic representation.

Energy balance

An overview of the energy partitioning into the distinct molecular degrees of freedom during fs-laser induced associative desorption of D_2 from Ru(001) is given in Table 3.1. The energies are expressed in terms of a temperature which neglects the statistical weight of the different degrees of freedom and is thus well-suited to judge if non-thermal energy partitioning is present. In addition, the rate-weighted adsorbate temperature $T_{\mathrm{ads}}^{\mathrm{RW}}$ for a laser fluence of $\langle F \rangle = 85\,\mathrm{J/m^2}$ applied in the experiments is denoted.

The total energy of the desorbing particle flux along the surface normal for an ensemble of diatomic molecules is given by [Kol94]

$$\langle E_{\mathrm{flux}} \rangle = \langle E_{\mathrm{trans}} \rangle + \langle E_{\mathrm{vib}} \rangle + \langle E_{\mathrm{rot}} \rangle = 2k_{\mathrm{B}}T_{\mathrm{trans}} + k_{\mathrm{B}}T_{\mathrm{vib}} + k_{\mathrm{B}}T_{\mathrm{rot}}. \tag{3.2}$$

Under full thermal equilibrium between all molecular degrees of freedom of the D_2 molecule under formation and the Ru(001) surface, the energy content in every degree of freedom can be represented by the *same* temperature $T_{\mathrm{ads}}^{\mathrm{eq}}$, leading to a total energy in the desorption

translation	T_{trans}	$\langle E_{\mathrm{trans}} \rangle / 2k_{\mathrm{B}} =$	2500 K
vibration	T_{vib}	$\langle E_{\mathrm{vib}} \rangle / k_{\mathrm{B}} =$	1200 K
rotation	T_{rot}	$\langle E_{\mathrm{rot}} \rangle / k_{\mathrm{B}} =$	910 K
modeled	$T_{\mathrm{ads}}^{\mathrm{RW}}$		1800 K

Table 3.1.: Overview of the energy partitioning into the different molecular degrees of freedom during the fs-laser induced D_2 recombination. The energies are expressed in terms of temperatures to take into account the different statistic weight of the degrees of freedom. The rate-weighted (RW) adsorbate temperature $T_{\mathrm{ads}}^{\mathrm{RW}}$ is obtained from a weighting procedure explained in the text and illustrated in Fig. 3.9.

flux according to Eq. (3.2) of $\langle E_{\mathrm{flux}}^{\mathrm{eq}} \rangle = 4k_{\mathrm{B}}T_{\mathrm{ads}}^{\mathrm{eq}}$. Note that this simplified energy balance does not take dynamical corrections due to steering mechanisms or barriers in activated processes or coupling to phonons into account. Assuming $\langle E_{\mathrm{flux}}^{\mathrm{eq}} \rangle = \langle E_{\mathrm{flux}} \rangle$, one can now derive $T_{\mathrm{ads}}^{\mathrm{eq}} = \langle E_{\mathrm{flux}} \rangle / 4k_{\mathrm{B}}$ and with the experimental results for T_{trans}, T_{vib} and T_{rot} obtains a value for $T_{\mathrm{ads}}^{\mathrm{eq}} = 1780\,\mathrm{K}$. This is in excellent agreement with the modeled $T_{\mathrm{ads}}^{\mathrm{RW}}$ of 1800 K. Provided that the assumption of full thermal accommodation is correct, it seems as if the friction model is capable to describe the energy content in the desorbing D_2 molecule flux. Bearing in mind that $T_{\mathrm{ads}}^{\mathrm{RW}}$ results from a constant, one-dimensional and time-independent frictional coupling coefficient η_{el}, these matching temperatures appear rather astonishing and have to be discussed carefully as will be done further below.

It has to be noted that the energy content in the external and internal degrees of freedom was measured for an ensemble of D_2 molecules desorbing perpendicular to the Ru(001) surface. This means that the above presented considerations may fall short in the case of a significantly broad angular distribution of the desorbing particles, i.e. for molecules leaving the surface under angles different from the normal direction. On the other hand, the successful description and modeling of the investigated desorption process suggests that a rather peaked angular desorption distribution of the D_2 molecules should be expected, but which yet needs to be verified experimentally.

Unequal energy partitioning

It is obvious that a one-dimensional friction model which describes the energy content in the D_2 desorption flux surprisingly successfully, is not suited to make statements about an unequal energy transfer into different degrees of freedom of the emerging molecule. As can be seen from Table 3.1, such an unequal energy partitioning is observed and the ratio between translational, vibrational and rotational temperatures describing the energy content in the corresponding degrees of freedom is determined to be 2.7:1.3:1. This means that the fs-laser induced associative desorption of hydrogen from a saturation covered Ru(001) surface results in D_2 molecules with a predominantly translational excitation.

In contrast, equal energy partitioning between the different degrees of freedom is expected for non-activated reactions under full equilibrium conditions with the surface. This type of reactions was extensively investigated in permeation experiments, where atomic hydrogen permeates through a Pd(100) single crystal and desorbs associatively from the surface [Sch92, Wet01]. The translational, vibrational, and rotational temperatures of the desorbing particle

flux have been determined as a function of the surface temperature. The expected equal energy partitioning was generally observed, whereby small deviations from complete equilibrium could be attributed to dynamical corrections as rotational cooling and vibrational heating[3].

Since such an equilibration is obviously not observed in the present scenario, it has to be discussed, if the observed unequal energy partitioning is either due to the anisotropic non-adiabatic activation of the reaction or the result of an activated process governed by the ground state PES. First, the peculiarities of the non-adiabaticity will be considered: Hot-electron driven desorption of a *molecular* adsorbate like CO or NO initiated by fs-laser pulses reveal high vibrational temperatures T_{vib} of the desorbing molecules ranging from $\approx 1300\,\mathrm{K}$ [Str96] to $\approx 2200\,\mathrm{K}$ [Pry90]. In both cases only moderate translational temperatures T_{trans} have been observed, so that an unequal energy partitioning towards an enhancement of vibrational excitation results. The energy partitioning expressed in terms of $T_{\mathrm{trans}}{:}\,T_{\mathrm{vib}}$ is $1:3.7$ for NO desorbing from Pd(111)[4] [Pry90] and $T_{\mathrm{trans}}{:}\,T_{\mathrm{vib}}{:}\,T_{\mathrm{rot}}$ is $1:6.2:1$ for the CO desorption from Cu(100) [Str96]. The high T_{vib} reflect the high electronic temperatures due fs-laser excitation of the metal substrate. The highly excited electrons couple more efficiently to the intramolecular stretch vibration than to the center-of-mass motion [Avo89, Kin98, Tul00] (see also Section 1.1.4). The vibrational excitation remains rather undamped in the desorption exit channel and is therefore preserved into the gas phase. In addition, dynamical cooling discussed for the CO/Cu(100) case may lead to a lowering of translational temperatures increases the inequality of energy partitioning. This effect is based on the short interaction time during the desorption process. The desorbing molecule leaves the surface without complete equilibration with the heat bath of the solid. The degree of freedom responsible for desorption is the center-of-mass motion perpendicular to the surface so that this dynamical cooling mainly affects T_{trans}.

The efficient coupling between metal surface electrons and the intramolecular stretch vibration of a *molecular* adsorbates like NO or CO points towards the multi-dimensionality of non-adiabatic coupling with respect to the molecular degrees of freedom and the resultant unequal energy partitioning. This means that energy is not transferred into a single coordinate with a single coupling constant, but via different channels and with different coupling strengths which additionally depend on the velocities and positions of the involved atoms as explained in Appendix A. Recent, *ab initio* calculations on the frictional electronic coupling for the dissociative adsorption of H_2 on Cu(111) and the associative desorption of N_2 from Ru(001) by Luntz et al. [Lun05] indeed reveal anisotropic friction coefficients between the normal and the lateral adsorbate coordinate. In these activated systems, the electronic coupling near the adsorption minimum shows an anisotropy towards a considerably larger coupling into the z coordinate perpendicular to the surface with respect to the interatomic separation coordinate d. In both cases, this implies an initially strong adsorbate-substrate vibration, whereas the lateral movement is less excited in the beginning of the recombination process. This could be a possible reason for the observed unequal energy partitioning. Very recent calculations performed by Luntz et al. [Lun06] for the investigated femtosecond laser induced hydrogen

[3] Since in contrast to rotational cooling, vibrational heating is not discussed in Section 1.1.2, a short explanation is given: The strong lowering of the H_2 vibrational frequency at the surface results in an population of the vibrationally excited $v = 1$ state, which is higher than expected for a gas phase molecular ensemble of the same temperature. Therefore, a higher T_{vib} is required to describe the energy content in the vibrational degree of freedom, which is named vibrational heating [Gro96a].

[4] In this study, the strongly non-thermal rotational state population could not be represented by a single temperature and is therefore not considered in the given energy ratio.

recombination will be discussed in detail in Section 3.4.

Having explained the possible influences of the electron mediated reaction mechanism concerning unequal energy partitioning, a consideration of the topology of the electronic ground state PES follows. The ground state PES governing the hydrogen recombination on a hydrogen covered Ru(001) surface is calculated by Luntz et al. [Lun06] and depicted in the right panel of Fig. 3.1. An early barrier of $V^* \approx 60\,\mathrm{meV}$ is apparent in the entry channel to adsorption, which is consistent with the extrapolated minimum translational energy obtained from the TOF results discussed in Section 3.2.1. If no energy is exchanged between the light D_2 molecules and the heavy surface atoms as the molecules come down the barrier V^*, the potential energy of the barrier is released into the desorbing particle flux, leading to an increased energy content of $\langle E_{\mathrm{flux}} \rangle = \langle E_{\mathrm{flux}}^{\mathrm{eq}} \rangle + V^*$, where $\langle E_{\mathrm{flux}}^{\mathrm{eq}} \rangle$ denotes the energy content in the particle flux equilibrated with the Ru(001) surface. The successful description of the experimental data via $\langle E_{\mathrm{flux}} \rangle = \langle E_{\mathrm{flux}}^{\mathrm{eq}} \rangle$ does not evidence such an additional energetic contribution in the energy balance. On the other hand, steering mechanisms leading to rotational cooling can result in molecules desorbing with an energy smaller than $\langle E_{\mathrm{flux}}^{\mathrm{eq}} \rangle$. The overpopulation of rotational states with $J'' \leq 6$ in $v'' = 0$ suggests such an dynamical process. This means that the successful description of $\langle E_{\mathrm{flux}} \rangle$ within the one-dimensional friction model might be due to two compensating effects, namely rotational cooling and and the crossing of a translational barrier.

One has to note that a distinction between a possible anisotropic electronic excitation and unequal energy partitioning due to the topology and the multi-dimensionality of the ground state PES is beyond the scope of the performed experimental investigations. Dynamical trajectory simulations involving multi-dimensional friction coefficients of the different sections

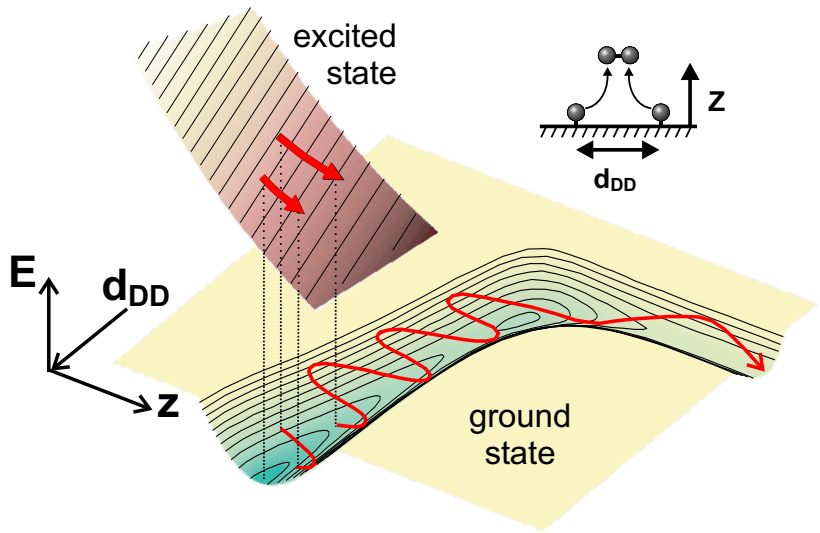

Figure 3.11.: Illustration of the fs-laser induced associative desorption of D_2 from Ru(001). Coordinates denote the center-of-mass distance z of D_2 from the surface and the intramolecular bond length $d_{\mathrm{D\text{-}D}}$. The electron mediated reaction mechanism is visualized in the diabatic representation by multiple transitions to an electronically excited PES which is only of qualitative character. An exemplary trajectory demonstrates a possible route which results in predominantly translational excitation. The ground state PES is adapted from Luppi et al. [Lup].

of the PES are required to distinguish the possible scenarios.

Figure 3.11 summarizes the experimentally obtained understanding of the fs-laser induced associative desorption of hydrogen from Ru(001). The depicted PESs are restricted to two dimensions z and $d_{\text{D-D}}$, taking into account the molecular degrees of freedom into which the most energy is transferred. The multiple electronic excitation mechanism revealed by Denzler et al. [Den04] is visualized by multiple transitions to a very schematic electronically excited PES. A possible reaction trajectory is suggested, in which an initially rather strong excitation of the z coordinate of the atomically bound adsorbates normal to the Ru(001) surface leads to a predominantly translational excitation of the reaction product after turning around the elbow. No effort is made to visualize dynamical effects resulting from the ground state PES, which might also be responsible for the observed unequal energy partitioning into the different molecular degrees of freedom.

3.4. Comparison with "first principle" dynamics

As mentioned in the discussion of the experimental results, dynamical trajectory calculations including multi-dimensional friction coefficients along the reaction trajectory are required to distinguish the possible sketched scenarios leading to the measured unequal energy partitioning. Luntz et al. [Lun06] performed such calculations, and the discussion of their outcome is subject of this section.

The underlying theoretical approach is based on molecular dynamics with electronic frictions [Hea95] in the nearly adiabatic limit, where the motion of the adsorbate is governed by the electronic ground state PES and the electronic excitations are considered by frictional and fluctuating forces (Section 1.1.4). Both, the PES and the friction coefficients are obtained from "first principle" density functional theory (DFT) calculations, so that there are *no adjustable* parameters in the comparison of the calculations with experiments. The intramolecular bond length d and the molecular center-of-mass distance z are considered as well as a single phonon coordinate q describing the coupling to the lattice. A detailed description is given in Appendix A.

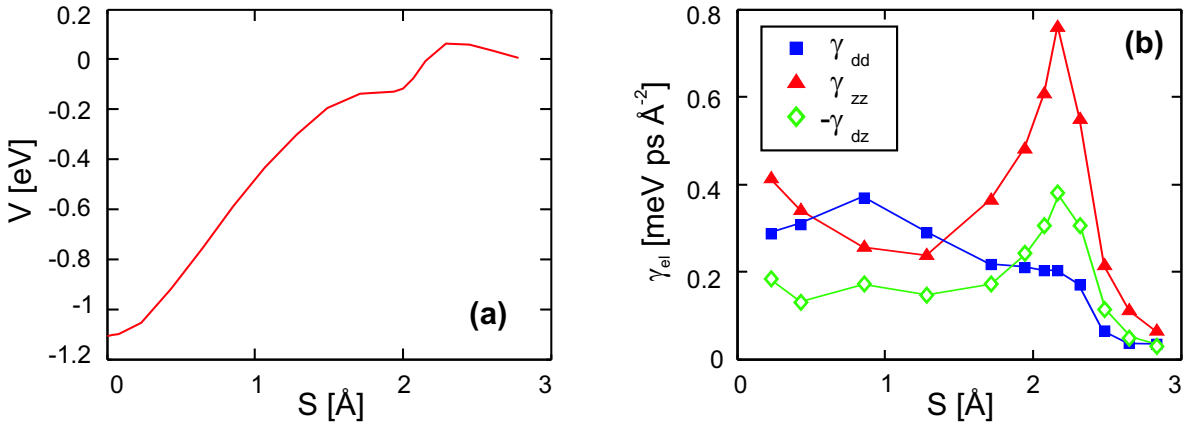

Figure 3.12.: (a) DFT potential energy projected along the minimum energy path for desorption S. S=0 corresponds the (1×1)H:Ru(001) absorbed state and S=3 corresponds to the H_2+Ru:H asymptote. (b) Electronic friction coefficients along the minimum energy path for desorption S. Figures from [Lun06].

The calculated PES is depicted in the panel of Fig. 3.1, and its peculiarities have been already discussed concerning the unequal energy partitioning. The DFT potential energy along the minimum energy path S towards desorption is depicted in Fig. 3.12(a) and the discussed barrier is apparent. The components of the two-dimensional friction coefficient[5] γ_{el} along S are depicted in Fig. 3.12(b). γ_{el} is rather isotropic ($\gamma_{dd} \approx \gamma_{zz}$) for small S. However, $\gamma_{zz} \approx 3\gamma_{dd}$ at larger S due to the peaking of γ_{zz} near the translational barrier. This peaking behavior at the transition state was also observed in earlier studies investigating the gas surface dynamics of H_2 with Cu(100) and N_2 with Ru(001) [Lun05] and seems to be a quite general phenomenom. γ_{el} is not only calculated for the minimum energy reaction path S, but as a function of intramolecular distance d and the center-of-mass distance z to the Ru(001) surface leading to $\gamma_{el} = \gamma_{el}(d, z)$.

[5] Note that the friction coefficient γ_{el} is related via Eq. (1.45) to the inverse frictional coupling η_{el} discussed in the framework of the applied friction model.

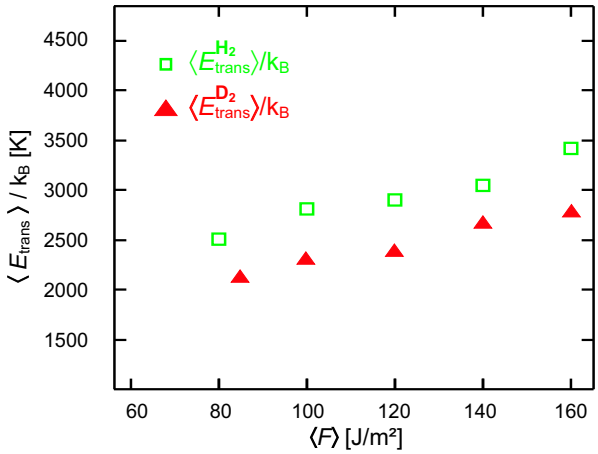

Figure 3.13.: Translational energies $\langle E_{\mathrm{trans}} \rangle = T_{\mathrm{trans}} / k_{\mathrm{B}}$ of desorbed H_2 and D_2 calculated by the dynamic model as a function of absorbed laser fluence [Lun06].

The fs-laser induced associative desorption dynamics were then determined using molecular dynamics with electronic frictions [Hea95]. The underlying classical equations of motion are discussed in Appendix A. Several thousand trajectories are averaged. In the following the outcome of these trajectory calculations will be presented and compared to the experimental results.

The two-pulse correlation, fluence dependence and the isotope effect concerning the desorption yield (see Section 3.1.2) are very well reproduced by the dynamical model [Lun06], but will not be discussed in greater detail. The calculated mean translational energy as a function of absorbed laser fluence is plotted in Fig. 3.13. $\langle E_{\mathrm{trans}} \rangle$ is expressed in terms of $T_{\mathrm{trans}} = \langle E_{\mathrm{trans}} \rangle / k_{\mathrm{B}}$, which allows comparison with the experimental results[6]. The dynamics reproduce the experimentally observed trend (see Fig. 3.5) and the isotope effect with higher T_{trans} for the lighter molecule very well. The absolute values of T_{trans} are somewhat lower ($\approx 500\,\mathrm{K}$) than in the experiment. A linear extrapolation of T_{trans} to $\langle F \rangle = 0$ gives an intercept of $\approx 1400\,\mathrm{K}$, which is also in good agreement with the experiment.

The energy partitioning obtained by projecting the desorbed D_2 (H_2) total energy onto vibrational and translational coordinates is given by

$$\langle E_{\mathrm{tot}} \rangle = \langle E_{\mathrm{trans}} \rangle + \langle E_{\mathrm{vib}} \rangle = k_{\mathrm{B}} T_{\mathrm{trans}} + k_{\mathrm{B}} T_{\mathrm{vib}}. \tag{3.3}$$

T_{vib} increases linearly with $\langle F \rangle$, but always with $T_{\mathrm{trans}} > T_{\mathrm{vib}}$ as observed in the experiment. The difference $\langle E_{\mathrm{trans}} \rangle - \langle E_{\mathrm{vib}} \rangle \approx 70 \pm 20\,\mathrm{meV}$ is constant for all fluences in the dynamic model. Modeling of purely thermal associative desorption (see Appendix A) also results in the same unequal energy partitioning [Lun06]. This means that the observed unequal energy partitioning between vibrational and translational coordinates occurs because of propagation on the ground state PES and not due to anisotropic electronic frictional coupling as speculated in Section 3.3. The unequal energy partitioning, $\langle E_{\mathrm{trans}} \rangle - \langle E_{\mathrm{vib}} \rangle \approx 70 \pm 20\,\mathrm{meV}$, is quite close to the activation barrier V^* of the PES which is predominantly along the translational

[6] The difference in dimensionality between the experiment and the dynamic model leads to the factor of two between the modeled and measured energies due to phase space considerations. Therefore, the corresponding temperatures T_{trans} are discussed.

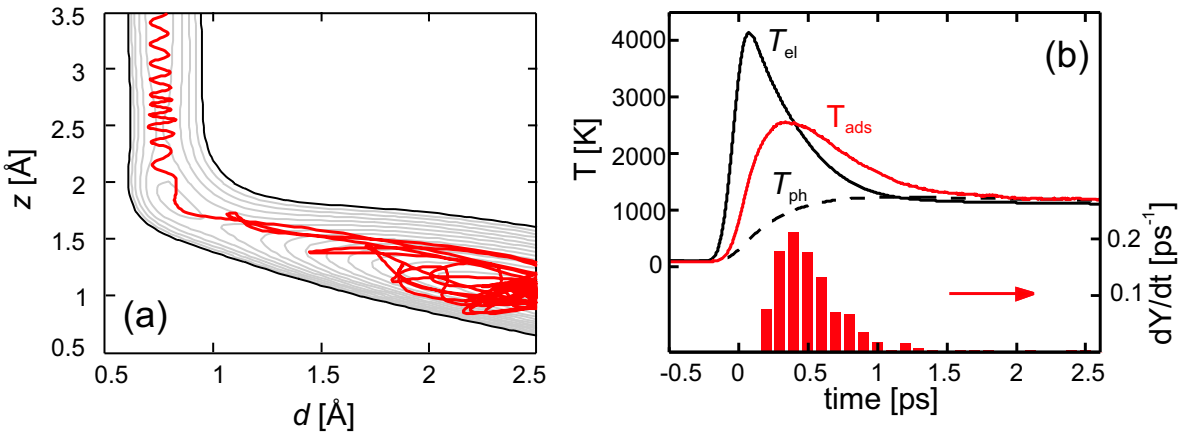

Figure 3.14.: (a) Associative desorption trajectory for H_2 following an adsorbed laser fluence of $140\,\mathrm{J/m^2}$ overlayed on the 2D PES. (b) Transient electron and phonon temperatures T_{el} and T_{ph} after fs-laser excitation with $\langle F \rangle = 120\,\mathrm{J/m^2}$. The adsorbate temperature $T_{\mathrm{ads}} = \langle E_{H_2} \rangle / 2k_{\mathrm{B}}$ is obtained by averaging over 6000 trajectories. The bar graph is the induced rate of desorption $\mathrm{d}Y/\mathrm{d}t$ as a function of time t. Figures taken from [Lun06].

coordinate (see Fig. 3.1). No knowledge about the origin of the smaller energy partitioning into the rotational coordinates nor the observed alignment is obtained, since these coordinates are not included in the dynamic model.

As a final point, the astonishing success of the 1D friction model describing the multi-dimensional associative desorption of hydrogen from Ru(001) will be discussed in the light of the analysis of the desorption trajectories calculated by Luntz et al. [Lun06]. An exemplary trajectory is shown in Fig. 3.14(a).

As is obvious, a rapid interchange between between z and d coordinate takes place. This justifies the assumption of equipartition between the two degrees of freedom which then together with averaging over thousands of trajectories allows to use a transient adsorbate temperature $T_{\mathrm{ads}}(t) = \langle E_{H_2}(t) \rangle / 2k_{\mathrm{B}}$ depicted in Fig. 3.14(b) together with phonon and electron temperatures T_{ph} and T_{el}, respectively, and the desorption rate $\mathrm{d}Y(t)/\mathrm{d}t$. E_{H_2} represents the molecular energy and is given by $E_{H_2} \approx E_{\mathrm{tot}} - E_q$, where E_{tot} is the total energy of the system and E_q is the energy projected onto the nearly separable phonon coordinate. Note that $\mathrm{d}Y(t)/\mathrm{d}t$ peaks when T_{ads} peaks and that there is a delay between this peak and the initial fs-laser excitation. Thus, the maximal desorption rate occurs after T_{el} has substantially cooled. The delay between the fs-laser and maximal desorption rate measures the average time it takes the H-H system to climb out of the adsorption well and is approximately equal to the half width of the 2PC correlation width which means that for this system the 2PC measures essentially the H_2 desorption time.

Inspection of the individual trajectories and the transient desorption rate in Fig. 3.14(b) indicate that most of the hot electron excitation of nuclear coordinates occurs when the system is still deep in the H-H adsorption well and much below the barrier. In this region, although $\gamma_{dd} \approx \gamma_{zz}$, most of the nuclear excitation occurs through the vibrational coordinate because of the four times smaller reduced mass along d relative to z. By the time the H-H approaches the barrier (where $\gamma_{zz} \gg \gamma_{dd}$), T_{el} has cooled so that the electronic excitation is small. However, even though most of the excitation occurs through the vibrational coordinate, the rapid interchange between z and d coordinates during the desorption trajectory gives little

memory of the mode of excitation.

Comparing Fig. 3.14(b) with Fig. 3.9, one clearly notices the qualitatively similar shape of $T_{\mathrm{ads}}(t)$ in both graphs resulting from completely different theoretical approaches. This similarity originates from the rapid interchange between z and d and is the fundamental reason for the success of the 1D model in reproducing most aspects of the hot electron induced associative desorption.

3.5. Summary

Energy transfer to the different degrees of freedom during the hot electron mediated associative desorption of hydrogen from a saturation covered Ru(001) was investigated. The energy transfer to the internal molecular degrees of freedom was determined via resonance enhanced multi-photon ionization (REMPI). Rotational quantum state populations in the vibrational ground state and the first excited state were measured and yield average rotational energies of $\langle E_{\mathrm{rot}} \rangle / k_{\mathrm{B}} = 800$ and 1500 K, respectively, for an absorbed laser fluence of $\langle F \rangle = 85\,\mathrm{J/m^2}$. In addition, a mean vibrational energy of the desorbing molecules is extracted which amounts to $\langle E_{\mathrm{vib}} \rangle / k_{\mathrm{B}} = 1200\,\mathrm{K}$. Investigations of the molecular alignment reveal that a *helicopter*-like rotation is favored by the desorbing molecules.

Extensive time-of-flight (TOF) measurements reveal a pronounced isotope effect with higher translational energies $\langle E_{\mathrm{trans}} \rangle$ for the lighter isotope and show a strong dependence of $\langle E_{\mathrm{trans}} \rangle$ on fluence $\langle F \rangle$. $\langle E_{\mathrm{trans}} \rangle / 2k_{\mathrm{B}}$ ranges from 2000 to 3200 K for $\langle F \rangle$ between 50 and $140\,\mathrm{J/m^2}$. The isotope effect and the trend of the increasing translational energies could both be qualitatively described by a 1D friction model. The higher electronic temperatures due to stronger laser excitation and a more efficient electronic coupling to the lighter isotope explain the experimental findings.

Knowledge about the energy transfer to all molecular degrees of freedom for an absorbed laser fluence $\langle F \rangle = 85\,\mathrm{J/m^2}$ allows to denote the energy partitioning which expressed in terms of $T_{\mathrm{trans}} : T_{\mathrm{vib}} : T_{\mathrm{rot}}$ is $2.7 : 1.3 : 1$. No unambiguous explanation of the origin of this unequal energy partitioning could be made based on the experimental results and, thus, it was speculated if this unequal partitioning results from either anisotropic electronic coupling or from dynamic propagation on the ground state PES.

Insight into the origin of the unequal energy partitioning is obtained from a theoretical "first principle" investigation performed by Luntz et al. [Lun06], which describe the hot-electron mediated fs-laser induced hydrogen recombination. They show that the unequal energy partitioning is due a translational barrier on the ground state PES and that the unequal energy partitioning should be also observed for thermal desorption. Furthermore, they revealed that the success of the 1D friction model is based on rapid intermixing between the two considered molecular coordinates in the early stage of the desorption process, which allows to describe the energy content in the adsorbate by a *single* coordinate.

The astonishing success of the applied 1D model in yielding the correct energy content of the desorbing particle flux is therefore most likely due to two compensating effects: an increase of $\langle E_{\mathrm{trans}} \rangle$ because of the translational barrier upon desorption and rotational cooling resulting in a lowered rotational energy.

In summary, the fs-laser induced associative desorption of hydrogen from a saturation covered Ru(001) surface can be described as follows: The reaction is electron mediated and the molecular coordinates interchange rapidly upon desorption which gives little memory of the molecular mode of electronic excitation. The observed energy partitioning can be assigned to the topology of the ground state PES which exhibits a translational barrier leading to an excess of translational energies of the desorption flux in the gas phase.